Biofouling, February 2004 Vol 20 (1), pp 1–23

Taylor & Francis
Taylor & Francis Group

Quantifying Biofilm Structure: Facts and Fiction

HALUK BEYENAL[a], ZBIGNIEW LEWANDOWSKI [a,b,*] and GARY HARKIN[c]

[a]*Center for Biofilm Engineering, Montana State University, Bozeman, MT 59717, USA;* [b]*Department of Civil Engineering, Montana State University, Bozeman, MT 59717, USA;* [c]*Computer Science Department, Montana State University, Bozeman, MT 59717, USA*

(Received 30 July 2003; in final form 27 November 2003)

There is no doubt among biofilm researchers that biofilm structure is important to many biofilm processes, such as the transport of nutrients to deeper layers of the biofilm. However, biofilm structure is an elusive term understood only qualitatively, and as such it cannot be directly correlated with any measurable parameters characterizing biofilm performance. To correlate biofilm structure with the parameters characterizing biofilm performance, such as the rate of nutrient transport within the space occupied by the biofilms, biofilm structure must first be quantified and expressed numerically on an appropriate scale. The task of extracting numerical parameters quantifying biofilm structure relies on using biofilm imaging and image analysis. Although defining parameters characterizing biofilm structure is relatively straightforward, and multiple parameters have been described in the computer science literature, interpreting the results of such analyses is not trivial. Existing computer software developed by several research groups, including ours, for the sole purpose of analyzing biofilm images helps quantify parameters from biofilm images but does nothing to help interpret the results of such analyses. Although computing structural parameters from biofilm images permits correlating biofilm structure with other biofilm processes, the meaning of the results is not obvious. The first step to understanding the quantification of biofilm structure, developing image analysis, methods to quantify information from biofilm images, has been made by several research groups. The next step is to explain the meaning of these analyses. This presentation explains the meanings of several parameters commonly used to characterize biofilm structure. It also reviews the authors' research and experience in quantifying biofilm structure and their attempts to quantitatively relate biofilm structure to fundamental biofilm processes.

Keywords: biofilms; biofilm structure; biofilm modeling; image analysis

INTRODUCTION: THE NEED FOR QUANTIFYING BIOFILM STRUCTURE

The desire to quantify biofilm structure from images taken with the aid of traditional light microscopes or laser confocal scanning microscopes arose soon after biofilm researchers discovered that biofilm structure affects the rate of nutrient transport to the deeper layers of biofilms and, ultimately, controls microbial activity and the rate of biofilm accumulation. Detailed studies have since documented that biofilm structure determines the mass transport mechanism in the space occupied by the biofilm and mass transport rates near and within biofilms (Lawrence *et al*., 1991; Caldwell *et al*., 1992; Lewandowski *et al*., 1993a; 1993b; deBeer *et al*., 1994a; 1994b; Zhang & Bishop, 1994a; Bishop & Rittmann, 1995; Yang & Lewandowski, 1995; Bishop, 1997). Since the structures of biofilms are visually different, it is expected that these differences reflect the magnitude of environmental factors that control biofilm accumulation, microbial composition, hydrodynamics, the chemical composition of the solution, the chemical and physical properties of the surface supporting biofilm growth, and the fundamental processes occurring in biofilms, *viz.* attachment, detachment, and growth.

Thus far, most of the effects that biofilm structure has on biofilm processes are hypothetical, and they will remain so until tools are developed to quantify biofilm structure and to correlate the structure with the intensity of the processes that the structure is believed to influence or reflect. Quantifying the

*Corresponding author; fax: 1 - 406 - 994-6098; e-mail: ZL@erc.montana.edu

ISSN 0892-7014 print/ISSN 1029-2454 online
DOI: 10.1080/0892701042000191628

relations between biofilm structure and biofilm processes will open new avenues in biofilm research as biofilm structure not only affects biofilm processes but also is a testimony to the history of biofilm formation and thus can be used to determine past events that occurred during biofilm formation. For example, it is known that biofilms grown at high shear stress develop elongated microcolonies (Lewandowski & Stoodley, 1995). It is also known that dense biofilms develop either as a result of high shear stress or as a result of starvation (Beyenal & Lewandowski, 2000). Therefore, if a researcher samples an unknown biofilm having high density, the shape of the microcolonies may resolve whether the density has increased as a result of starvation or as a result of exposing the biofilm to a high shear stress.

Much effort in biofilm research has been dedicated to determining the factors that affect biofilm structure, and some progress has been made in understanding these factors. For example, Van Loosdrecht *et al*. (1995) discuss the effects of substrate loading rate, shear stress, and growth rate on biofilm structure. In recent studies completed in the authors' laboratory (Tanyolac & Beyenal, 1997; Beyenal *et al*., 1998; Beyenal & Lewandowski, 2000; 2002), it is postulated that biofilm development follows a simple strategy that optimizes two goals, *viz*. i) survival of the biofilm on the surface and ii) maximizing the transport of nutrients to the deep layers of the biofilm. Biofilms may sacrifice the efficiency of nutrient transport to remain on the surface. Biofilm structure appears to be important enough to warrant its presence in future mathematical models of biofilm accumulation and activity, so that relations among biofilm structure, rate of biofilm accumulation, and microbial activity in biofilms can be quantified within the same framework of mathematical models.

One important conclusion drawn from studying the relationship between biofilm structure and function is that the complexity of biofilm processes defeats the reductionistic approach to biofilm studies. The cause-and-effect relations between biofilm structure and fundamental biofilm processes, *viz*. attachment, detachment, and growth, are impossible to isolate because they form feedback loops. For example, hydrodynamics affects biofilm structure and biofilm structure affects hydrodynamics. This complex web of relationships, which are impossible to isolate and very difficult to quantify, together with the lack of suitable mathematical models that accept biofilm structure as a control parameter, defeat the attempts of embedding biofilm structure within the framework of mathematical modeling of biofilm processes. Because of their inherent complexity, it is possible that the relations between biofilm structure and biofilm processes eventually will have to be treated using methods of nonlinear dynamics. Meanwhile, however, biofilm researchers and practitioners need a workable system that can be used to quantify biofilm structure and to relate it to biofilm activity. This quest for simple models that could improve understanding of system performance is particularly important to environmental engineers who design biofilm reactors and need to understand the relations between biofilm structure and performance of biofilm reactors. Such knowledge would be valuable in water treatment industry, to mitigate the deleterious effect of biofilms on membrane processes. Existing concepts call for extending the lifetime of filtration membranes by manipulating the structure of the accumulated biofilms. Without precise knowledge of how biofilm structure responds to stresses it is impossible to design a process of manipulating biofilm structure to achieve the desired effect.

Before proceeding toward quantifying biofilm structure, it is important to define two terms, *viz*. biofilm structure and biofilm heterogeneity. The term biofilm structure was initially used by biofilm researchers when referring to the physical structure of biofilms (morphology), and it was considered self-explanatory. However, as time progressed, many authors started to use this term as a synonym for heterogeneity when implicitly referring to various kinds of heterogeneities in biofilms, *i.e*. physiological, chemical, and genetic. Thus the meanings of the terms biofilm structure and biofilm heterogeneity overlapped. Since the term biofilm structure is no longer self-explanatory, it must be defined every time it is used. For the purpose of this paper, the authors accept the initial meaning of biofilm structure, *viz*. the distribution of biomass in the space occupied by the biofilm. The term biofilm heterogeneity is used when referring to the non-uniform distribution of any feature within the space occupied by the biofilm, *e.g*. non-uniform distributions of biomass, chemistries, or physiological groups of microorganisms are called structural heterogeneity, chemical heterogeneity, and physiological heterogeneity, respectively.

Many authors have concluded that biofilm structure needs to be quantified, and they have developed relevant experimental procedures for monitoring biofilm structure and calculating parameters characterizing biofilm structure. These contributions generally fall into one of the following categories: i) comparing the structures of biofilms (*e.g*. Heydorn *et al*., 2002; Purevdorj *et al*., 2002); ii) testing the reproducibility of biofilm structure (*e.g*. Heydorn *et al*., 2000b; Jackson *et al*., 2001); iii) monitoring temporal variations in biofilm structure (*e.g*. Lewandowski *et al*., 1999; Heydorn *et al*., 2002; Pereira *et al*., 2002); iv)

testing the effects of various substances, including antimicrobials, on biofilm structure (*e.g.* Christensen *et al*., 2001); v) quantifying the effects of environmental factors on biofilm structure (Pereira *et al*., 2002; Lewandowski & Beyenal 2003a); vi) computing parameters characterizing biofilm structure for biofilm modeling or using biofilm structure in biofilm modeling (Rittmann *et al*., 1999; van Loosdrecht *et al*., 2002).

Parameters characterizing biofilm structure are typically computed from biofilm images taken using some type of microscopy. The best for this purpose is confocal laser microscopy because it allows the acquisition of images of fully hydrated biofilms at high spatial resolution not only in the lateral direction, which traditional light microscopy allows, but also in the vertical direction. Many authors use image analysis to compute parameters characterizing biofilm structure, and some design their own software to perform such analyses automatically. Some obvious parameters to compute are fractal dimension, which characterizes the variability of biofilm structures, and areal porosity, which characterizes void coverage. Some researchers, including the authors' group, calculate more exotic parameters such as energy or textural entropy, which originated from research in computer science. Although many parameters are potentially useful for quantifying biofilm structure, their relationships to biofilm processes are yet to be determined.

Many attempts have been made to give meaning to the structural features of biofilms. The following section gives an account of recently published reports that analyze biofilm structure. Zahid and Ganczarczyk (1994) calculated fractal dimensions and areal porosities of RBC biofilms using the bioquant Meg-IV software (R&M Biometrics, USA). Hermanowicz *et al*. (1995) computed fractal dimensions from images of heterotrophic biofilms using MOCHA Image Analysis Software (Jandel Scientific, San Rafael, California) and IDL Interactive Data Language (Research System Incorporated, Boulder, Colorado). Kuehn *et al*. (1998) designed a computer program to perform automated quantification of biofilm structure using image acquisition and image analysis, and to calculate biovolume from these images. Recently, Pereira *et al*. (2002) used the software of Kuehn *et al*. (1998) to compare the effects of laminar and turbulent flow regimes on the characteristics of *Pseudomonas fluorescens* biofilms. Ji *et al*. (2000) developed software which automatically calculates fractal dimension from biofilm images using the Euclidean distance map, the Minkowski sausage method (dilation), the box counting method, the corner method (counting and perimeter), the fast method (regular and hybrid), the parallel lines method, the cumulative intersection method, and the mass radius (short and long) methods. Heydorn *et al*. (2000a) developed a versatile software (COMSTAT) to calculate biovolume, surface area coverage, biofilm thickness distribution, mean biofilm thickness, the volumes of micro-colonies, fractal dimension, roughness coefficient, average and maximum distance, and surface-to-volume ratio from a three-dimensional stack of biofilm images. The authors used this software to compare the structures of biofilms and to test the reproducibility of *Pseudomonas aeruginosa* biofilms (Heydorn *et al*., 2000b). Kjelleberg and Molin (2002) used COMSTAT to quantify the roughness of *P. aeruginosa* biofilms. Heydorn *et al*. (2002) used COMSTAT to monitor the development of a four-strain *P. aeruginosa* biofilm and compare biofilm structures. Recently Mah *et al*. (2003) used COMSTAT to compare architecture of wild and mutant *P. aeruginosa* biofilms. Daims *et al*. (2001) developed software to quantify the number of cells from digitized images of microbes subjected to fluorescence *in situ* hybridization (FISH) with rRNA-targeted oligonucleotide probes. Later, Dionisi *et al*. (2002) used the software of Daims *et al*. (2001) and quantified the effect of the solids retention time (SRT) of ammonia- and nitrite-oxidizing bacteria. Lomander *et al*. (2002) developed an image analysis tool and computed the biofilm coverage and circularity of cell clusters for *E. coli* K12 biofilms grown on glass, polished 316 stainless steel, and brushed 316 stainless steel.

Recognizing the importance of quantifying biofilm structure, the authors' research group has developed software, called the Image Structure Analyzer (ISA), to calculate textural entropy, homogeneity, energy, areal porosity, average horizontal and vertical run lengths, diffusion distance, and fractal dimension from digital biofilm images (Yang *et al*., 2000). To make the results of image analysis less dependable on the operator, an automatic thresholding algorithm has also been developed and integrated with the ISA (see Yang *et al*., 2001). The ISA automatically quantifies parameters from biofilm images and can perform batch processes, which is important when the number of images is large.

The performance of the ISA has been tested by several researchers. Lewandowski *et al*. (1999) used the ISA to monitor temporal variations in the structure of biofilms composed of *P. aeruginosa* (ATCC 700829), *P. fluorescens* (ATCC 700830), and *Klebsiella pneumoniae* (ATCC 700831) and concluded that as time progresses some of the structure parameters may reach stable values. Lewandowski (2000) used it to calculate areal porosities of layered biofilms and developed a method for calculating volumetric biofilm porosity. Jackson *et al*. (2001) used the ISA to test the reproducibility of biofilm structure in mixed culture biofilms and concluded that only biofilms grown for short time periods (a

few days) have reproducible structure. Christensen *et al*. (2001) used the ISA to test the effects of alginate-degrading enzyme (AlgL) on pure culture biofilms of *P. aeruginosa* (strains 8830 and ATCC 700829) and mixed population biofilms composed of *P. aeruginosa* (ATCC 700829), *P. fluorescens* (ATCC 700830), and *K. pneumoniae* (ATCC 700831) and concluded that AlgL did not degrade the tested biofilms. Beyenal and Lewandowski (2001) used the ISA to quantify the areal porosity and fractal dimension of mixed population bacterial biofilms composed of *Desulfovibrio desulfuricans* and *P. fluorescens* and concluded that the extent of biofilm heterogeneity was directly correlated with the flux of H_2S from the cell clusters. Purevdorj *et al*. (2002) used the ISA to quantify the areal porosity, fractal dimension, average horizontal run length, average diffusion distance, textural entropy and energy of biofilms of wild-type *P. aeruginosa* PAO1 and cell-cell signaling using lasI mutant PAO1-JP1 under laminar and turbulent flows, and concluded that both cell signaling and hydrodynamics influenced biofilm structure. Lewandowski *et al*. (2004) tested reproducibility of long-term biofilms and discussed existence of steady state biofilm structure using the numerical parameters extracted from biofilm images and concluded that biofilms did not reach steady state, which raised questions about using the concept of steady state to model biofilm processes.

Relating Biofilm Structure to Fundamental Biofilm Processes: the Concept of Discretized Biofilms and its use in Relating Biofilm Structure and Activity

The main problem with using parameters quantified from biofilm images is the lack of an appropriate mathematical framework that relates these parameters to the rate of biofilm accumulation and activity. Addressing this problem the authors have developed the concept of discretized biofilms (Beyenal & Lewandowski, 2000; Lewandowski & Beyenal, 2003b). The basic premise for the concept is that biofilms can be divided into units, and that each of these can be studied separately and the behavior of the entire biofilm can be predicted by integrating the information obtained from the individual units. To discretize the biofilms, they are divided into a finite number of layers parallel to the substratum. There are other ways of discretizing biofilms, *e.g*. using individual microcolonies as biofilm units. Although this approach is useful in many biofilm studies, its use in biofilm modeling leads to difficulties when the information from the individual units needs to be integrated; it is neither practical nor possible to study all the microcolonies of a biofilm, and it is not known which microcolony is 'average.' This difficulty is avoided by dividing a biofilm into layers and using these as biofilm units because each feature measured within a layer can be averaged, the number of the layers is finite, and all layers can be evaluated as part of a single measurement.

Since parameters computed from biofilm images should be useful in modeling biofilms to have scientific merit, some approach for selecting useful parameters objectively is needed. The structural elements of the biofilm that might be chosen to measure are called features. Biomass cluster size and shape are examples of features. Structural features are visual, and possess characteristics such as size, shape, color and texture that may be expressed quantitatively. One measure of the relevance of a feature is how well it correlates with changes in the underlying biofilm environment, *e.g*. local concentrations of relevant chemicals. Another alternative is to choose features that may be correlated with biofilm function, if the function is well defined and can be measured. It is reasonable to believe that the size of biomass clusters or interstitial spaces might be associated with variations in species or nutrition, and that the shape of clusters might be associated with hydrodynamics. Features that cannot be related to underlying biological, chemical or physical processes will probably not lead to scientific insights.

To provide a recognizable goal for the image analysis, it is conjectured that there exist a finite number of features that describe the structure of a biofilm and that these contain enough information either to reflect variations in the growth dynamics or to predict the functional characteristics of the biofilm. As a starting point for finding such features, it is hypothesized that two kinds of information can be obtained from a digital biofilm image, *viz*. i) textural information showing variations in gray level which can be caused by local density, thickness and color variations in biofilms, and ii) areal information showing the size and orientation of cell clusters. Computing these parameters from biofilm images does not guarantee that the parameters are good descriptors of the biofilm. Whether a parameter is relevant has to be decided later, using separate criteria that are specific to the process under study. For example, to characterize biofilm response to varying nutrient supply it may be important to monitor biofilm porosity, while characterizing biofilm response to varying shear stress may require measuring parameters related to biomass cluster shape.

Once descriptors of biofilm structure (parameters) have been selected, they are tested for relevance by embedding in biofilm models of activity or accumulation. If a link to known biofilm

processes cannot be made, it is difficult to justify the use of the parameter. The existing models of structurally heterogeneous biofilms (Wimpenny & Colasanti, 1997; Picioreanu *et al*., 1998a; 1998b; 2000, 2001; Hermanowicz, 2001) are mostly based on cellular automata and commonly suffer from the difficulty of relating the theoretical development to the experimental verification. This difficulty seems to be directly related to the fact that these models are artificial constructs, and that their principles consider individual microbial cells as biofilm units, and are therefore incompatible with most results derived from studying conditions in real biofilms, which tend to average the results over a certain area or a certain biofilm volume. It is also not clear whether individual microbial cells should be considered as biofilm units. In contrast, discretizing biofilms by dividing them into layers is fully compatible with the results delivered by the major tools used in biofilm research, *i.e*. microsensors to evaluate biofilm activity, chemical concentrations, local densities, local effective diffusivities, and confocal microscopy to evaluate biofilm structure (Figure 1).

Data collected from biofilms must be reproducible but long-term biofilm processes are notoriously difficult to reproduce. To avoid problems related to biofilm reproducibility two strategies are in use, *viz*. i) studying very young biofilms that have accumulated for a few hours to a few days only, and ii) running biofilm experiments only once. The first approach trades reproducibility for relevance because natural biofilms are usually older than a few days. This approach can be applied to questions relevant to the initial events of biofilm formation but not to questions relevant to long-term biofilm accumulation. The second approach conceals and ignores the problem of reproducibility. The authors have developed a series of procedures and tests used as quality assurance for generating reproducible biofilm processes. Although complete success has not been achieved, progress has been made, as is reported in the following sections.

GROWING BIOFILMS AND TAKING IMAGES

The importance of using well-documented procedures to grow biofilms cannot be overemphasized; the object of the analysis, the biofilms, have to be grown reproducibly to make the results of image analysis meaningful. It is important to grow biofilms in reactors that permit control of hydrodynamics and mass transfer as biofilm structure depends on the hydrodynamics and on the availability of nutrients. The reactors must provide researchers with the ability to measure parameters such as flow velocity and calculate Reynolds number, and shear stress. A large number of biofilm reactors have been described in the literature. Some are available commercially, but most are made by the researchers. The authors grow biofilms in a specially designed flat-plate, open channel reactor. Such reactors have been found to be useful because they allow investigators to control the hydrodynamics, to make microelectrode measurements, and to collect biofilm images; the images are taken through the bottom and the microsensors are introduced through the top of the reactor. Unless special construction is required, the reactor is a polycarbonate channel, 2.5 cm wide,

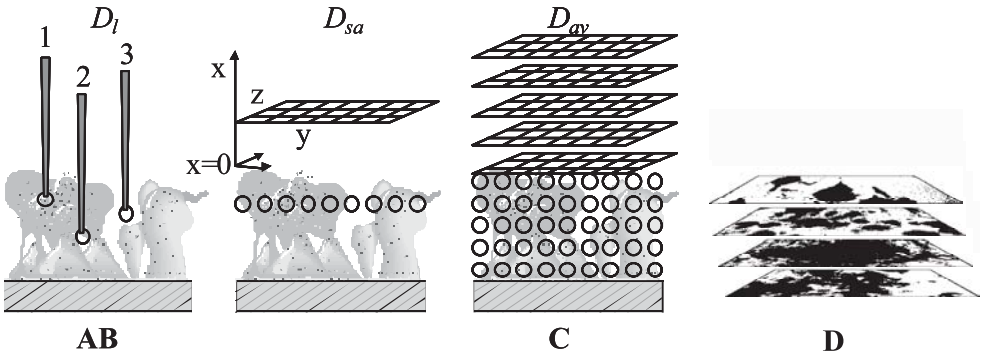

FIGURE 1 Discretized biofilms: implementation of the concept. The example in this figure shows distribution of diffusivity within a biofilm measured by microelectrodes. (A) Local relative effective diffusivities (D_l) are measured by microelectrodes at arbitrarily selected locations at different distances from the bottom. This procedure generates profiles of diffusivity which are relevant only at the locations where they were measured, vary widely between locations, and therefore are of minor use as a descriptor of biofilm diffusivity. An improved procedure allows averaging diffusivities at defined distances from the bottom. (B) The D_l are measured at grid points equally distant from the bottom. The measured D_l are then averaged, which gives the surface-averaged relative effective diffusivity, $D_{sa} = \sum_{n=1}^{k} D_{ln}/k$. (C) The average relative effective diffusivity, $D_{av} = \sum_{n=1}^{p} D_{san}/p$, is an average of all local measurements for the entire biofilm. In a similar manner, chemical concentrations such as dissolved oxygen can be measured and averages computed for each layer. (D) A series of confocal images of a biofilm taken at the same level where microelectrode profiles were taken.

4.0 cm deep and 34.5 cm long. The bottom of the reactor is made of glass to improve image quality. The procedures used by the authors to grow biofilms in flat-plate reactors are described in Jackson *et al*. (2001). Figure 2 shows a diagram of the experimental setup.

Biofilm images taken using a digital camera connected to a computer *via* a frame grabber are saved as TIFF files. Because RGB images are composed of red, green and blue, we commonly convert the images to gray scale images (Figure 3). Each pixel in the gray scale image corresponds to an integer between 0 and 255 reflecting the intensity of the light.

From the gray scale images two classes of parameters are calculated: i) textural and ii) areal. Although these parameters quantify biofilm structure, in most instances it is not clear how they are related to the fundamental biofilm processes of attachment, detachment, and growth. Except for a few parameters, such as areal porosity and fractal dimension, it is not immediately clear how these parameters are related to specific biofilm processes, and they are therefore relevant. To determine whether a computed parameter is relevant, it is monitored in various biofilms, and correlated with biofilm activity and the rate of biofilm accumulation. In principle, the authors do not have any preconceived notions about the relevance of any of the parameters that are computed. Rather, it is expected that, with time, when enough experimental data have been accumulated, the structural parameters measured in various biofilms will be corrleated with the intensity of biofilm processes

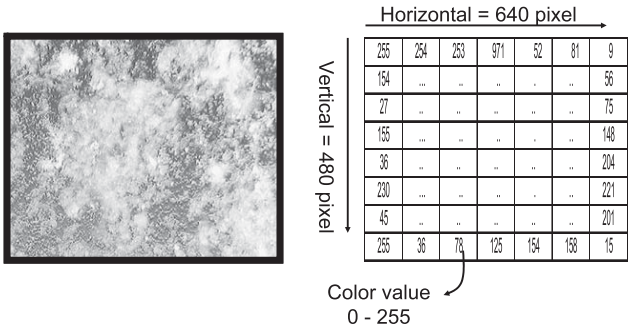

FIGURE 3 A gray scale biofilm image (left); each pixel has an intensity value represented by a number between 0 and 255. For image analysis, horizontal and vertical directions are described (right), as well as the image size. The image size is 640 × 480 pixels and the bright and dark areas show cell clusters and voids, respectively.

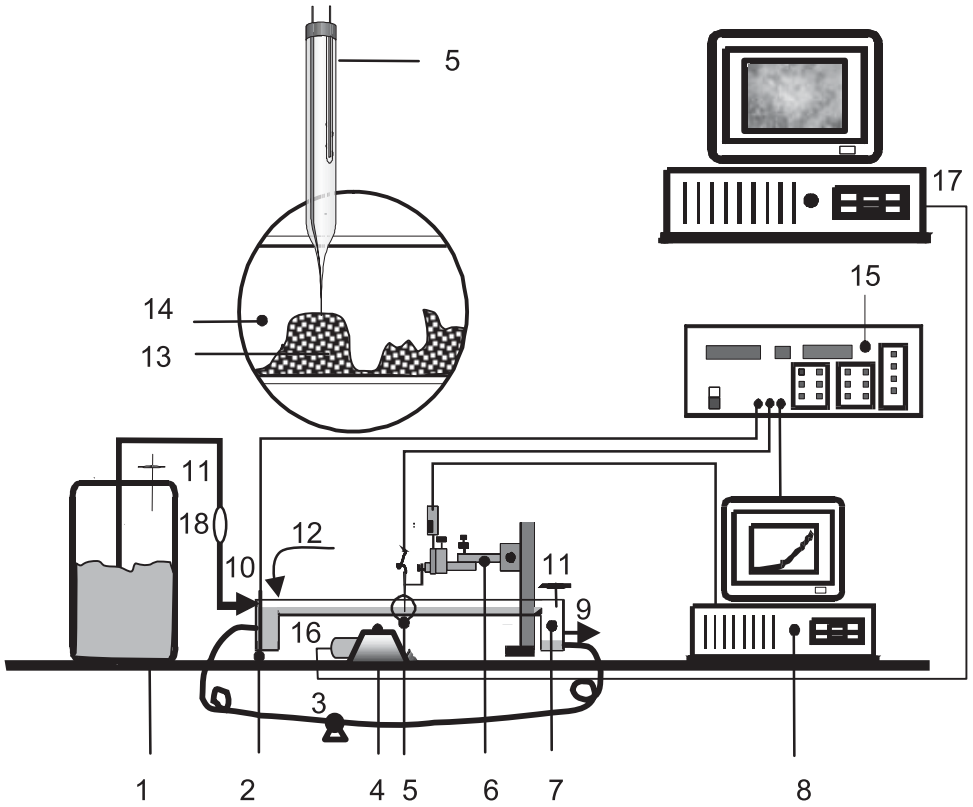

FIGURE 2 Experimental setup used to grow biofilms, take biofilm images, and measure biofilm activity using microelectrodes. 1 = growth medium; 2 = reference electrode*; 3 = peristaltic pump and recycle loop; 4 = inverted microscope; 5 = microelectrode*; 6 = micromanuplator*; 7 = flat plate reactor; 8 = computer* to control microelectrode position and measure chemical concentration; 9 = outflow; 10 = fresh feed; 11 = air filter; 12 = filtered air inlet; 13 = cell cluster; 14 = interstitial void; 15 = picoammeter*; 16 = digital camera; 17 = computer to acquire biofilm images; 18 = flow breaker; * these instruments were used only during the measurements, not during routine reactor operation.

measured independently in the same biofilms, to determine the relevance of the computed parameters.

COMPUTING PARAMETERS FROM BIOFILM IMAGES

Textural Parameters

Texture, described as a repeating pattern of local variations in image intensity (Yang *et al*., 2000), provides information about the spatial distribution of intensity levels in a neighborhood. In computer science literature, texture is often used to partition images into regions of interest and classify those regions.

Textural parameters quantify biofilm structure by comparing the size, position, and/or orientation of the visual components. Each textural parameter measures the character of the cell clusters and interstitial spaces based on the likelihood that pixels of similar or dissimilar types would be neighbors. In their analyses the authors calculate the following textural parameters described by Haralick *et al*. (1973): i) textural entropy; ii) energy (angular second moment); iii) homogeneity (inverse difference moment).

The calculations described here are based on descriptions given by Haralick *et al*. (1973), and the textural parameters are computed from the gray level co-occurrence matrix (GLCM). This matrix contains information about the positions of pixels having similar gray level values, and it is computed from the spatial dependence matrices computed for the horizontal and vertical directions. Horizontal and vertical spatial dependence matrices show intensity variations for their respective directions.

The terms energy and entropy when used in reference to images are somewhat confusing, particularly to life scientists who immediately associate them with the laws of thermodynamics and Claussius's entropy. However, the terms energy and entropy are used in other sciences, and their meanings are analogous to those used in thermodynamics, but not identical. In image analysis the term energy was introduced by Haralick *et al*. (1973), as a measure of directionally repeating patterns of pixels. The term entropy is also used in other sciences. Entropy in communication, defined by Shannon in 1948 (a mathematical theory on communication), measures uncertainty of information, and increasing entropy is associated with the loss of information. Energy and entropy in sciences other than thermodynamics are dimensionless. The following section defines energy and entropy when used in reference to images.

Calculating the Normalized Spatial Dependence Matrix

The following example shows an image as a 4×4 matrix with four gray scale levels (0–3).

0	0	1	1
1	2	0	1
2	3	1	0
2	2	2	3

The horizontal spatial dependence matrix (P_H) of this image is calculated as:

$$P_H = \{p_H(a,b)\} = \begin{bmatrix} p_H(0,0) & p_H(0,1) & p_H(0,2) & p_H(0,3) \\ p_H(1,0) & p_H(1,1) & p_H(1,2) & p_H(1,3) \\ p_H(2,0) & p_H(2,1) & p_H(2,2) & p_H(2,3) \\ p_H(3,0) & p_H(3,1) & p_H(3,2) & p_H(3,3) \end{bmatrix} = \begin{pmatrix} 2 & 3 & 1 & 0 \\ 3 & 2 & 1 & 1 \\ 1 & 1 & 4 & 2 \\ 0 & 1 & 2 & 0 \end{pmatrix}$$

where p_H (a, b) is the number of changes in the gray scale from a-to-b in adjacent horizontal locations in the image moving in either direction. For example, p_H (0, 1) is the number of changes in the gray scale from 0 to 1 in the horizontal direction. There are two such changes moving from left-to-right and one moving from right-to-left for a total of three. Because direction is not considered, the matrix is symmetrical around the diagonal.

Similarly, the vertical spatial dependence matrix (P_V) is:

$$P_V = \{p_V(a,b)\} = \begin{bmatrix} p_V(0,0) & p_V(0,1) & p_V(0,2) & p_V(0,3) \\ p_V(1,0) & p_V(1,1) & p_V(1,2) & p_V(1,3) \\ p_V(2,0) & p_V(2,1) & p_V(2,2) & p_V(2,3) \\ p_V(3,0) & p_V(3,1) & p_V(3,2) & p_V(3,3) \end{bmatrix} = \begin{pmatrix} 0 & 4 & 1 & 1 \\ 4 & 2 & 2 & 0 \\ 1 & 2 & 2 & 2 \\ 1 & 0 & 2 & 0 \end{pmatrix}$$

The spatial dependence matrix (P_{HV}) is the sum of the horizontal and vertical spatial dependence matrices:

$$P_{HV} = P_H + P_V = \{p_{HV}(a,b)\} = \begin{pmatrix} 2 & 7 & 2 & 1 \\ 7 & 4 & 3 & 1 \\ 2 & 3 & 6 & 4 \\ 1 & 1 & 4 & 0 \end{pmatrix}$$

where $p_{HV}(a,b)$ is the total number of intensity variations from a-to-b and b-to-a in the horizontal and vertical directions. Normalization is accomplished by summing the elements of the spatial dependence matrix and dividing each element by the sum.

$$\text{sum} = \sum_a \sum_b P_{HV}(a,b) = 48$$

$$P_N(a,b) = \frac{P_{HV}}{\text{sum}} = \begin{pmatrix} 0.0417 & 0.1458 & 0.0417 & 0.0208 \\ 0.1458 & 0.0833 & 0.0625 & 0.0208 \\ 0.0417 & 0.0625 & 0.1250 & 0.0833 \\ 0.0208 & 0.0208 & 0.0833 & 0 \end{pmatrix}$$

The textural parameters that can be defined from the GLCM ($P_N(a,b)$) are:

$$\text{Textural entropy, } TE = -\sum_{a,b} \sum_{P_N(a,b)\neq 0} P_N(a,b) \ln(P_N(a,b)) \quad (1)$$

$$\text{Energy, } \quad E = \sum_a \sum_b \{P_N(a,b)^2\} \quad (2)$$

$$\text{Homogeneity, } \quad H = \sum_a \sum_b \frac{1}{1+(a-b)^2} P_N(a,b) \quad (3)$$

In the present example, the computed parameters are: textural entropy = 2.51, energy = 0.094, homogeneity = 0.571.

Meaning of Textural Parameters

The meaning of the textural parameters and the procedures used to calculate them are explained using the images in Figure 4.

Textural entropy (TE) is a measure of randomness in the gray scale of the image. The higher the textural entropy, the more heterogeneous is the image. Figure 4A shows an image with no structure, composed of only white pixels, *i.e.* a void. The textural entropy computed for this image is zero, showing there is no tonal variation in the pixels or heterogeneity in the image. Figure 4B, C and D contain increasing numbers of pixel clusters and the textural entropy increases accordingly.

Energy (E) is a measure of directionally repeating patterns of pixels and it is sensitive to the orientation of the pixel clusters and the similarity of their shapes. Smaller energy values mean frequent and repeated patterns of pixel clusters, and a higher energy means homogeneous image structure, no repeated patterns. In Figure 4A, energy equals 1, showing that there are no repeating patterns in that image. However, as the number of repeating clusters increases, energy values decrease (Table I).

Homogeneity (H) is a measure of spatially repeating patterns of pixels. It measures the similarity of the clusters; a higher homogeneity indicates a more homogeneous image structure. Homogeneity is normalized with respect to the distance between changes in texture; it is independent of the locations of the pixel clusters in the image. In Figure 4A, homogeneity equals 1, showing there are no repeating spatial patterns in the image; the amount of homogeneity decreases with the increasing number of clusters (Table 1).

H *vs* E. The definitions of these two parameters are similar, and the meaning of these parameters needs further explanation. This may best be done by comparing the images in Figure 4. Figure 4C contains one more cluster than Figure 4B, and the additional cluster is shifted horizontally. Consequently, there is a pattern of repeating pixel clusters in the horizontal direction. However, the shapes of the two clusters are identical. Therefore, comparing the computed parameters, it is not surprising that the energy decreases more than the homogeneity ($\Delta E = 0.19$ and ($\Delta H = 0.06$). Indeed, ΔE is almost three times higher than (ΔH, showing that there is significant directional variation between the images in Figures 4B and those in 4C. Similarly, when Figures 4B and 4D are compared, $\Delta E = 0.59$ and ($\Delta H = 0.28$. This shows that the decrease in homogeneity is caused by the repeating pattern of pixel clusters, while the accompanying decrease in energy is caused by directional variations in the pattern of pixel clusters in these images.

Textural Parameters Computed from Real Biofilm Images

Two biofilm images are compared in Figure 5. Figure 5A shows large clusters, and Figure 5B shows small clusters. Textural parameters computed from these images are in given in Table II.

The biofilm in Figure 5A shows large clusters with small intensity variations, and it is expected that it has a lower TE than the biofilm in Figure 5B. Since more repeating micro-structures are seen in Figure 5B than in 5A, it is expected that E and H will decrease. The decrease in H is more pronounced than the decrease in E, showing that directionally repeating patterns (or cell clusters) are more dominant in Figure 5B.

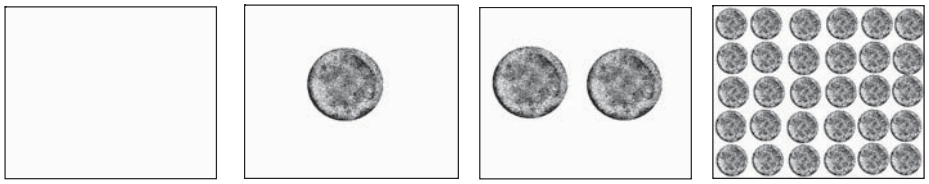

FIGURE 4 Custom generated images introducing textural parameters of images. A = white area; B = a single circular cell cluster; C = two cell clusters; D = many cell clusters. The textural parameters computed from these images are shown in Table I.

TABLE I The textural parameters computed for the images presented in Figure 4

Image	TE	E	H
4A	0	1	1
4B	0.60	0.78	0.94
4C	1.02	0.59	0.88
4D	1.97	0.19	0.66

TABLE II Textural parameters computed from the images in Figure 5

Image name	TE	E	H
5A	5.070068	0.01731	0.548574
5B	7.059066	0.003081	0.135297

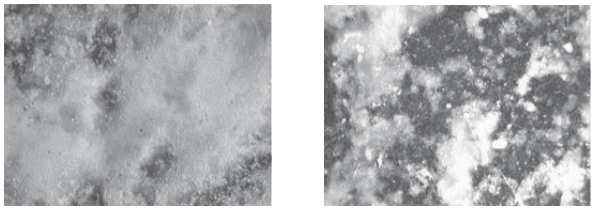

FIGURE 5 Two biofilms images which are analyzed verbally, below, and digitally, in Table II.

AREAL PARAMETERS

Areal parameters describe the morphology of biofilms, *i.e.* they are concerned with the size and shape/orientation of the constituent parts. Each parameter measures a unique characteristic feature of either the biomass or the interstitial space in the biofilm. Because of this, the first action that is performed in the image analysis is to separate cell clusters from interstitial voids. This is done by image segmentation (explained in detail in the section on the ''effect of thresholding'') which separates an image into distinct components. The parameters are initially computed using pixels rather than distances. However, since the pixels have known dimensions, the computed parameters can easily be converted to linear scales.

A common method of segmenting an image is known as thresholding, in which all pixels with gray levels below a particular value (the threshold) are changed to zero, and all above the threshold are changed to the maximum pixel value. The resulting black-and-white image has two visible components. The image in Figure 3 was converted to the black-and-white image shown in Figure 6.

Areal Porosity

The areal porosity (AP) is defined as the ratio of void area to total area:

$$\text{Areal porosity} = \text{AP} = \frac{\text{Number of void pixels}}{\text{Total number of pixels}} \quad (4)$$

Calculation of AP

In the following binary image, the number of void (zero) pixels is 27 and the total number of pixels is 36, so the areal porosity is $27/36 = 0.75$. This can be expressed as a percentage by multiplying the ratio by 100. The areal porosity of this image is thus 75%.

0	0	0	0	0	0
0	1	1	0	0	0
0	1	1	1	0	0
0	1	1	1	1	0
0	0	0	0	0	0
0	0	0	0	0	0

Average Run Length

The average run length is the average number of cell cluster pixels found consecutively in the image. Both the horizontal and the vertical average run length are used to provide additional information about directionality. These values provide a measure of the expected dimensions of a cell cluster and are therefore a measure of the average cluster size in their respective directions.

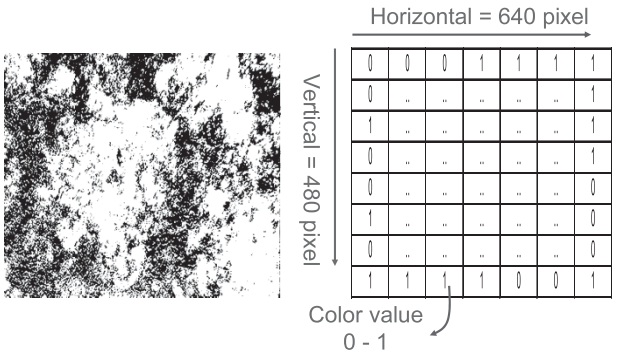

FIGURE 6 Binary image of a biofilm. When a gray scale biofilm image (see Figure 3) is converted to a binary level image, the intensity of the gray level is represented by a 1 or a 0 for each pixel. In the figure, black and white areas show cell clusters and voids respectively.

0	0	0	0	0	0	0
0	1	1	1	1	1	0
0	1	1	1	1	1	0
0	1	1	1	1	1	0
0	0	0	1	0	0	0
0	0	0	0	0	0	0
0	0	0	0	0	0	0

Number of horizontal runs = 4

0	0	0	0	0	0	0
0	1	1	1	1	1	0
0	1	1	1	1	1	0
0	1	1	1	1	1	0
0	0	0	1	0	0	0
0	0	0	0	0	0	0
0	0	0	0	0	0	0

Number of vertical runs = 5

Calculation of Average Run Length

Average horizontal or vertical run length is calculated by dividing the total number of pixels by the total number of runs in the horizontal or vertical direction. The above binary biofilm image has an average horizontal run length (AHRL) of (5 + 5 + 5 + 1)/4 = 16/4 = 4 (pixels) and an average vertical run length (AVRL) of (3 + 3 + 4 + 3 + 3)/5 = 16/5 = 3.2 (pixels). The total number of runs in the horizontal and vertical directions are 4 and 5, respectively. The total number of pixels is 16.

Average Diffusion Distance

The diffusion distance is defined as the minimum distance from a cluster pixel to the nearest void pixel in an image. Two diffusion distances are considered, average and maximum. The average diffusion distance (ADD) is the average of the minimum distance from each cluster pixel to the nearest void pixel over all cluster pixels in the image. A larger diffusion distance indicates a larger distance that substrate has to diffuse in the cell cluster. The maximum diffusion distance (MDD) is computed as the distance to the most 'remote' pixel in the cell cluster to the nearest void cluster.

The definition of diffusion distance refers only to the shortest distance, and does not specify how to calculate it. To calculate the ADD the Euclidean distance mapping algorithm (Breu *et al.*, 1995) is used. For the cluster cells that do not border void cells, the minimum distances from the cluster pixel to the nearest void pixel in the horizontal and vertical directions are calculated.

Calculation of ADD

The diffusion distance is the minimum distance from a biomass cell to interstitial space, and is intended to measure the distance to nutrients. An example of a diffusion distance calculation using Euclidean distance is shown below.

0	0	0	0	0	0
0	0	1	1	0	0
0	1	1	1	1	0
0	0	1	1	0	0
0	0	0	0	0	0

Original image

0	0	0	0	0	0
0	0	1	1	0	0
0	1	1.41	1.41	1	0
0	0	1	1	0	0
0	0	0	0	0	0

Euclidian distance map

The ADD is the average minimum distance over all the cells in a cluster. A slightly different measure is the MDD, which is the largest minimum distance of all the cells in the cluster. For example, in the above

image (Euclidian distance map), the average diffusion distance is the average of all distances = (1 + 1 + 1 + 1.41 + 1.41 + 1 + 1 + 1)/8 = 8.82/8 = 1.1 (pixels) and the MDD is 1.41.

Perimeter

The perimeter (P) is defined as the total number of pixels at the cell boundary, so only pixels in contact with interstitial space are counted.

0	0	0	0	0	0
0	0	1	1	0	0
0	1	1	1	1	0
0	0	1	1	0	0
0	0	0	0	0	0

The perimeter of the above image is 1 + 1 + 1 + 1 + 1 + 1 = 6. The shaded pixels are boundary pixels and the total number of these pixels is the perimeter.

Fractal Dimension

In fractal geometry, the two-dimensional fractal dimension (FD) measures the degree of irregularity in the perimeter of objects and varies between 1 and 2. The higher the FD value, the more irregular the perimeter of the object (Kaandorp, 1994). For the purposes of the present analysis, the higher the degree of variability in the biofilm cluster boundary, the higher the FD.

The Minkowski sausage method is used by the authors to calculate the FD (Russ, 2002), primarily because it relates naturally to image processing techniques. The Minkowski method measures the FD by determining the rate of change in the perimeter of an object as the thickness of the perimeter line is increased. Highly irregular perimeters will become shorter faster as the irregularities are smoothed by a thicker perimeter line. From an image processing viewpoint, dilation is used to accomplish the smoothing of the perimeter line. A circle of a particular radius sweeps the perimeter of the object, producing a new perimeter.

Specifically, the value of the boundary pixels is changed to zero and all other pixels to one (shown below), and then the Euclidean distance is calculated to obtain the distance to the boundary for each pixel. The dilation area is computed by varying the circle radius and counting the number of pixels at a distance smaller than this radius value. Then the perimeter is calculated as:

$$\text{Perimeter} = \frac{\text{Dilated area}}{\text{Diameter}} \tag{5}$$

Plotting the logarithm of the dilation circle diameter against the logarithm of the measured perimeter produces a straight line. The FD is defined as:

$$\text{Fractal dimension} = \text{FD} = 1 - \text{slope} \tag{6}$$

Calculation of FD

An example of calculating the FD is demonstrated for the binary image below.

0	0	0	0	0	0	0	0
0	0	0	0	0	1	1	1
0	0	0	0	0	1	1	1
0	0	0	0	1	1	1	1
0	0	0	0	0	1	1	1
0	0	0	0	0	0	1	1
0	0	0	0	0	0	0	0

1) Replace the boundary pixels with zeros and mark the rest with ones (see below).

1	1	1	1	1	1	1	1
1	1	1	1	1	0	0	0
1	1	1	1	1	0	1	1
1	1	1	1	0	1	1	1
1	1	1	1	1	0	1	1
1	1	1	1	1	1	0	0
1	1	1	1	1	1	1	1

2) Calculate the Euclidian distance map for the image generated in step 1 (see below).

5	4.12	3.16	2.24	1.41	1	1	1
4.47	3.61	2.83	2	1	0	0	0
4.12	3.16	2.24	1.41	1	0	1	1
4	3	2	1	0	0	1	1.41
4.12	3.16	2.24	1.41	1	0	0	1
4.47	3.61	2.83	2.24	1.41	1	0	0
5	4.24	3.61	2.83	2.24	1.41	1	1

To make this calculation easier the border pixels were replaced with zeros. It is also assumed that if

there is a cell cluster pixel at the border of the image, it will continue so the next pixel will not be a void.

3) Calculate the perimeter for each dilation; count the total number of pixels that have a distance < the radius of the dilation circle.

5	4.12	3.16	2.24	1.41	1	1	1
4.47	3.61	2.83	2	1	0	0	0
4.12	3.16	2.24	1.41	1	0	1	1
4	3	2	1	0	0	1	1.41
4.12	3.16	2.24	1.41	1	0	0	1
4.47	3.61	2.83	2.24	1.41	1	0	0
5	4.24	3.61	2.83	2.24	1.41	1	1

For a radius value of 1.5 pixels, the dilated area is 30 pixels (see above). To calculate the dilated area, the total number of pixels which have distances less than 1.5 (the dilation circle radius) are counted. The perimeter value is $30/3 = 10$.

4) Plot the logarithm of the diameter *vs* the logarithm of the perimeter and calculate the slope of the linear function as shown in Figure 7. Fitting the data to a line gives a slope value of -0.55, so the FD is $1 - (-0.55) = 1.55$.

The meaning of the FD is not clear unless some relationship between underlying processes and biomass surface irregularity can be found.

The Meaning of Areal Parameters

To expose the meaning of the areal parameters as was done for the textural parameters, a set of images are generated (Figure 8). Figure 8A shows a single cell cluster, 8B shows two clusters, 8C three, and 8D four cell clusters. The areal parameters computed from these images are given in Table III.

As seen in Table III, the ADD, MDD, AHRL and AVRL are the same for each image. This is expected since identical cell clusters should have identical ADD, MDD, AHRL and AVRL values, and the number of these cell clusters in the image is irrelevant. The perimeter value increased linearly with increasing number of cell clusters, as expected. Similarly, areal porosity decreased with increasing number of cell clusters.

Areal Parameters Computed from Real Biofilm Images

Two biofilm images are compared in Figure 9: Figure 9A shows a few small, elongated clusters and Figure 9B shows a single, less elongated cell cluster. The areal parameters computed from these images are given in Table IV.

Since image 9A has a few small, elongated clusters, it has a lower ADD than the ADD computed for the cluster in Figure 9B. The perimeters are close for these two images since the biofilms have the same amount of surface to transfer substrates (length of the edges). Since the biofilm in image 9A has a lower ADD a more efficient transfer of substrate over the shorter diffusion distance would be expected. Such analyses can be helpful in interpreting the results of chemical analyses of the bulk solution and in explaining differences in substrate consumption rates.

APPLICATIONS OF BIOFILM IMAGE ANALYSES

Biofilm researchers hope that the image analysis of biofilms will become a tool that allows the comparison of biofilms grown at different locations and under different growth conditions. It is not certain that this is realistic. The foundations of these expectations have been evaluated using related literature studies.

Comparing Structures of Biofilms

The first test was conducted to demonstrate that the structural parameters of developing biofilms change in a predictable manner. A biofilm composed of *P.*

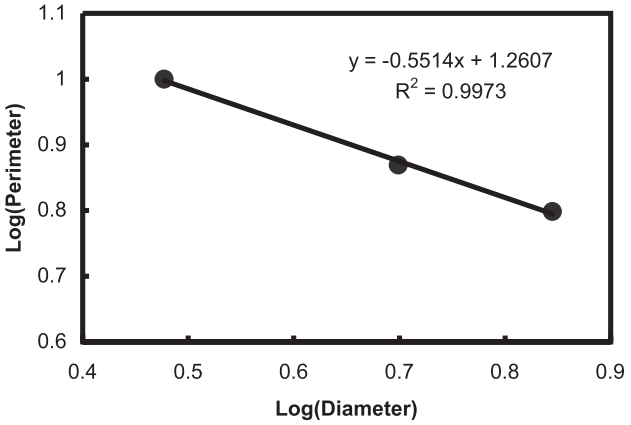

FIGURE 7 Log(diameter) *vs* Log(perimeter).

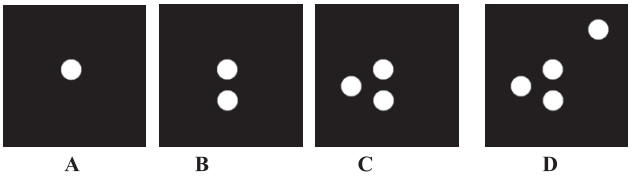

FIGURE 8 A = a single cell cluster; B = two cell clusters; C = three cell clusters; D = four cell clusters.

aeruginosa was grown in the flat-plate reactor with images of the biofilm taken through the bottom of the reactor, using light microscopy, at days 5 and 6 at exactly the same location, shown in Figure 10. The structural parameters were computed, and the results are given in Table V. These results are what might be expected. As time progressed areal porosity decreased as the cell clusters became larger. Textural entropy increased because of increased heterogeneity, while energy and homogeneity decreased because the cluster sizes and orientations changed. Although the cell clusters were expected to be changing, the left, bottom side of the image shows an attached cell cluster, which significantly influences the calculated parameters.

In this instance, the changes in the structural parameters appear to be related to the underlying processes. This simplistic example allows only the time to change, and it remains to be seen whether changing other factors (different biofilms and locations) can also provide useful comparative data.

Using structural features to compare biofilms is becoming popular, and using appropriate software developed for that purpose is the easiest way to compare structural parameters of various biofilms. Purevdorj *et al*. (2002) used ISA to quantify areal porosity, fractal dimension, average horizontal run length, average diffusion distance, textural entropy and energy of biofilms of wild-type *P. aeruginosa* PAO1 and the cell-cell signaling using lasI mutant PAO1-JP1 in biofilms grown in laminar and turbulent flows, and concluded that both cell-cell signaling and hydrodynamics influenced biofilm structure. Heydorn *et al*. (2002) used COMSTAT to quantify structural parameters from images of *P. aeruginosa* biofilms selecting average thickness and roughness coefficient as key parameters to quantify.

Monitoring Temporal Variations and Testing Biofilm Reproducibility

The second test statistically compared two biofilms grown under identical conditions. For this test, AP and temporal variations were monitored in two identically operated biofilm reactors inoculated with

TABLE III The computed areal porosity (AP), average diffusion distance (ADD), maximum diffusion distance (MDD), average horizontal run length (AHRL), average vertical run length (AVRL), and perimeter (P)computed from each image in Figure 8

Image	AP	ADD (pixels)	MDD (pixels)	AHRL (pixels)	AVRL (pixels)	P (pixels)
8A	0.983	9.65	27.46	44.02	44.80	160
8B	0.966	9.65	27.46	44.02	44.80	320
8C	0.949	9.65	27.46	44.02	44.80	480
8D	0.932	9.65	27.46	44.02	44.80	640

TABLE IV Areal parameters computed from the images in Figure 9

Image name	ADD (pixels)	MDD (pixels)	HRL (pixels)	VRL (pixels)	FD	P (pixels)	AP
9A	7.623214	36.35932	25.35278	49.46883	1.097069	1722	0.940579
9B	30.37936	102.4597	79.17414	152.7074	1.115244	1698	0.804642

Before the analysis the images were filtered using a 5(5 size median filter to remove noise

TABLE V Structural parameters computed from the images of the 5- and and 6-day-old biofilms shown in Figure 10

Figure/time	AP	FD	ADD (μm)	MDD (μm)	AHRL (μm)	AVRL (μm)	P (μm)	E	TE	H
10 A day 5	0.7828	1.245506	5.162522	38.26307	11.9867	13.48334	21085	0.0374	4.29007	0.5583
10 B day 6	0.5008	1.487203	12.02207	74.03546	19.67182	14.8541	36757.5	0.0076	5.28575	0.3252

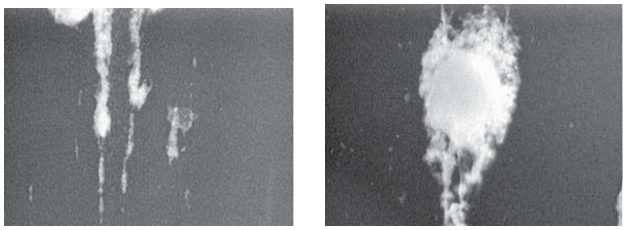

A B

FIGURE 9 Two biofilm images are compared verbally and digitally (Table IV).

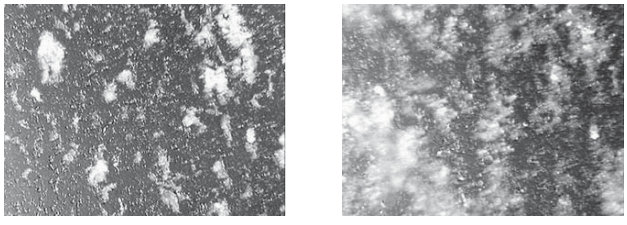

A **B**

FIGURE 10 A = an image of a biofilm acquired on the fifth day; B) = an image of exactly the same location on the biofilm acquired on the sixth day.

P. aeruginosa, *P. fluorescens*, and *K. pneumoniae*. The images were collected at the bottom level of the biofilm using light microscopy, so the results show AP at the bottom only (Figure 11). The general trend of the data in Figure 11 is as expected; as time progressed, the AP at the bottom of the biofilm decreased, showing more biofilm coverage.

Each data point in Figure 11 represents the average AP and standard deviation computed from 30 biofilm images acquired from each reactor. A two-tailed t-test was used to determine whether the two biofilms were statistically the same (Martinez & Martinez, 2002). The *p*-values are presented in Figure 12.

In a previous study conducted in the authors' laboratory, Jackson *et al*. (2001) quantified biofilm structures using AP, ADD, FD and TE to test biofilm structural reproducibility, and concluded that only biofilms grown for short time periods (a few days) had reproducible structure. Similarly, Heydorn *et al*. (2000b) compared biofilms using mean biofilm thickness as a key parameter, tested the reproducibility of *P. aeruginosa* biofilms and found that 6 d old biofilms were reproducible.

From the authors' studies, it appears that even biofilms grown under seemingly identical conditions show different patterns of growth. This conclusion is ominous, and raises questions about the validity of any process used to compare different biofilms based on their images. The test described here indicates that computing structural parameters from a biofilm is a valid tool for monitoring temporal changes in the biofilm structure but that using it as a tool to compare biofilms, even to compare biofilms grown under identical conditions in repeated experiments for longer periods, is questionable. It does not appear that there is a particular stage during biofilm accumulation that can be used to take representative images of the biofilm.

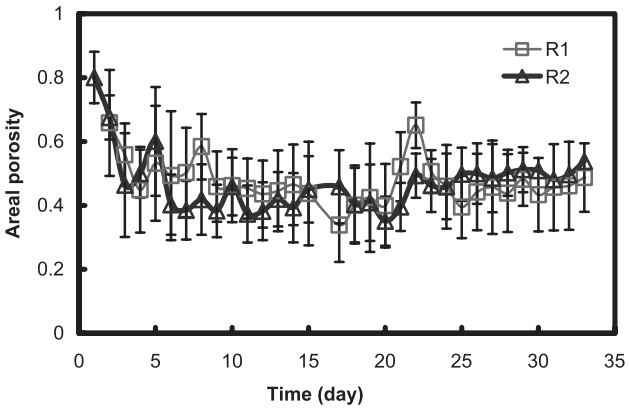

FIGURE 11 AP evaluated daily from 30 images taken randomly from each biofilm. R1 and R2 refer to the reactors, number one and number two.

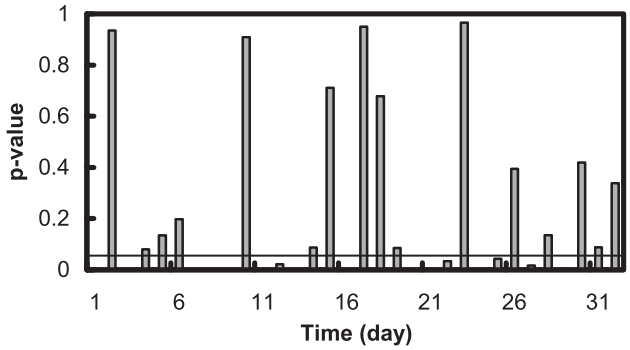

FIGURE 12 Statistical analysis, using the two tailed t-test, of areal porosities show that after about 6 d the identically inoculated and grown biofilms exhibited different growth patterns. The *p*-vales > 0.05 indicate that the biofilms were the same and the *p*-values < 0.05 indicate that the biofilms were different. The continuous horizontal line in Figure 12 marks the *p*-value of 0.05, which was accepted as the criterion for testing the null hypothesis.

Testing the Effect of Antimicrobials

To test the effect of antimicrobials on biofilm structure 5-day-old biofilms of *P. aeruginosa*, *P. fluorescens*, and *K. pneumoniae* were used. The biofilms were grown in a flat-plate reactor, and the images were collected through the bottom of the reactor. Figure 13 shows images before and 15 min after treatment, and the computed structure parameters are given in Table VI. The AP increased by 61% while ADD decreased 72% after treatment, showing that one of the effects of the antimicrobials was to decrease the average size of the microcolonies,

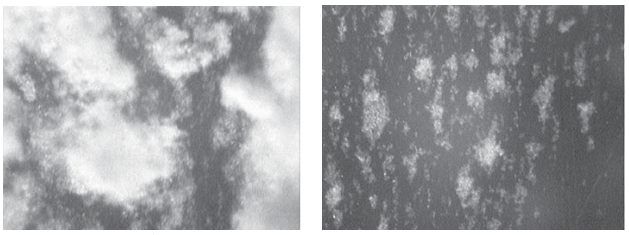

FIGURE 13 A = image of the biofilm taken before treatment; B = image after treatment.

TABLE VI Biofilm structural parameters before and after the treatment

Image	AP	FD	ADD (μm)	MDD (μm)	HRL (μm)	VRL (μm)	P (μm)	E	TE	H
13A Before	0.45	1.57	20.275	116.325	19.775	14.2375	36586.25	0.01324	6.99	0.116
13B After	0.74	1.56	3.275	27.4375	5.55	5.0375	47883.75	0.02931	6.35	0.117

which is also visible directly from the images in Figure 13. In this instance, the structural parameters accurately quantify the underlying biofilm process.

In one of the studies conducted in the authors' laboratory, Christensen *et al*. (2001) quantified biofilms structures before and after exposing to alginate-degrading enzyme (AlgL) and concluded that AlgL did not change the structures of the tested biofilms.

Quantifying Effects of Environmental Factors on Biofilm Structure

Temporal variations in biofilm structure can be monitored to evaluate the effects of various environmental factors on biofilm accumulation. For example, the effect of glucose concentration on biofilm structure will be shown. Biofilms of *P. aeruginosa, P. fluorescens*, and *K. pneumoniae* were grown in two flat-plate flow reactors operated at 10 cm s^{-1} flow velocity using 50 and 100 mg $l^{-1}$of glucose, respectively. The temporal variation in ADD of each biofilm is shown in Figure 14, where the ADDs increase as time progresses.

In another study, Lewandowski and Beyenal (2003a) quantified the effect of glucose concentration on the AP, and found that APs decreased when glucose concentration was increased. Pereira *et al*. (2002) quantified thickness and biovolume of biofilms grown at laminar and turbulent flow regime and found that the biofilms grown at laminar flow were thicker. Using image analysis to quantify the effects of various environmental factors on the structure of biofilms grown in laboratory reactors is probably the most promising use of this technique. Temporal variations in selected parameters quantifying biofilm structure are easily computed. It is not clear, however, which parameters should be used, and this can only be resolved using statistical analysis.

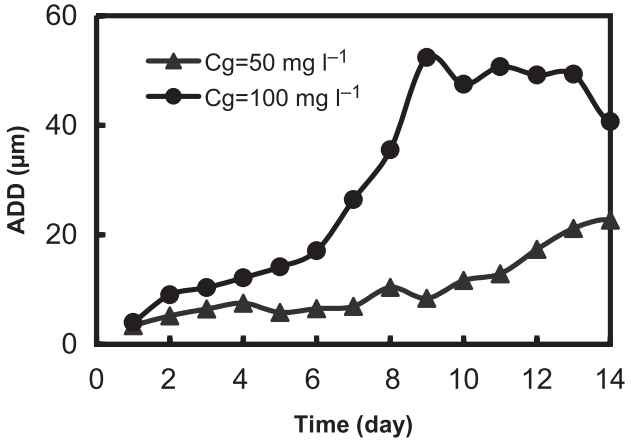

FIGURE 14 The variation in ADD by time for biofilms grown at a flow velocity of 10 cm s^{-1} and glucose concentrations of 50 mg l^{-1} (–▲–) and 100 mg l^{-1} (–●–). Each data point in the figure represents an average of 30 images acquired through the bottom of the reactor.

INTERFERING EFFECTS

Parameters computed from the images of biofilms are affected by the procedures used to acquire the images and by the procedure used to compute the parameters. Some of these effects are undesirable and difficult to control. In the following section several of these factors are presented and their effects demonstrated.

Linear Independence of Areal Parameters

Some of the areal parameters computed from biofilm images seem to be linearly related. If this can be demonstrated to be the case, eventually one of the related parameters is rejected as redundant. To understand the relationships among areal parameters, they can be evaluated for known shapes, such as circles. Figure 15 shows an example of such an analysis, the correlation of ADD with MDD, and AHRL and AVRL for circular cell clusters.

Some simple relations are valid in such analyses. For circles, AHRL/AVRL = 1 because the numbers of runs in the horizontal and vertical directions are the same. For a circle:

$$\mathrm{MDD} = 3 \times \mathrm{ADD} \tag{7}$$

These analyses often help in understanding results from computed real experiments. For example, in some experiments linear correlations between AHRL and AVRL have been noticed, which demonstrates the symmetrical nature of cluster growth. To further define the shape of the cell clusters, another useful parameter, the aspect ratio, has been defined:

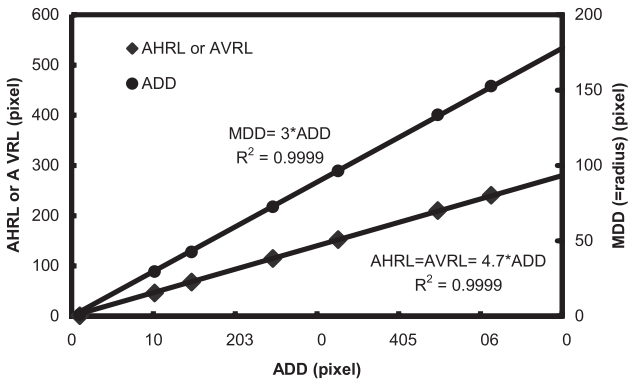

FIGURE 15 The variation in AHRL, AVRL and MDD with ADD for a circle. To obtain a different ADD the diameter of the circle is increased.

$$\text{Aspect ratio} = \frac{\text{AHRL}}{\text{AVRL}} \quad (8)$$

If the aspect ratio remains constant during biofilm growth, the biofilm microcolonies are growing symmetrically in the horizontal and vertical directions. If, however, shear stress, or any other action, tends to deform the microcolonies in one direction then this tendency is reflected by a changing aspect ratio.

Effects of Image Orientation and Image Reversing

Textural parameters reflect the distribution of gray scale intensity. Since it is spatially dependent, it is important to determine whether it is affected by image orientation. Figure 16A is rotated in Figure 16B and inverted in Figure 16C. The results are shown in Table VII.

All the textural parameters computed from the images shown in Figure 16A,B, and C are identical (TE = 5.6547, E = 0.0052, H = 0.3656), showing that the parameters are invariant with regard to orientation and chromatic inversion. This is important because simple image manipulations are common in the process of analyzing biofilm images. For example, textural parameters do not give useful information about the effect of flow rate on the cell clusters. Cell clusters become elongated in high-flow-rate environments, but the textural parameters can only detect repeating patterns of gray scale, which are not affected appreciably by the elongation. Such effects should be quantified using areal parameters.

The image rotation changes only the values of AHRL and AVRL. Reversing an image, on the other hand, affects all parameters because it replaces voids with cell clusters and *vice versa*.

Effect of Thresholding

As discussed earlier, thresholding is a segmentation method that compresses the color scale, typically to two colors. For biofilm images, thresholding is typically used to reduce 256 gray scale levels to two gray scale levels to separate the image into biomass and interstitial space. The operator arbitrarily selects one of the 256 gray scale levels as a threshold. Computer software then segments the image(s) into two parts with all gray levels less than or equal to the threshold becoming black and all higher gray levels becoming white.

To extract statistically meaningful morphological parameters from a series of images, the thresholding must be reproducible. The choice of threshold is subjective, so the choice of gray scale intensity selected to segment the images depends on the operator's understanding of the image content and the desired relationship between the two segments in the final image. The operator uses his or her best judgment and sets the gray scale level in such a way that the binary image appears to capture the essence of the biofilm structure. Since the parameters calculated from thresholded images depend on the selected gray scale level they also become subjective. Variability among operators in choosing the threshold adversely affects the measurements obtained from the

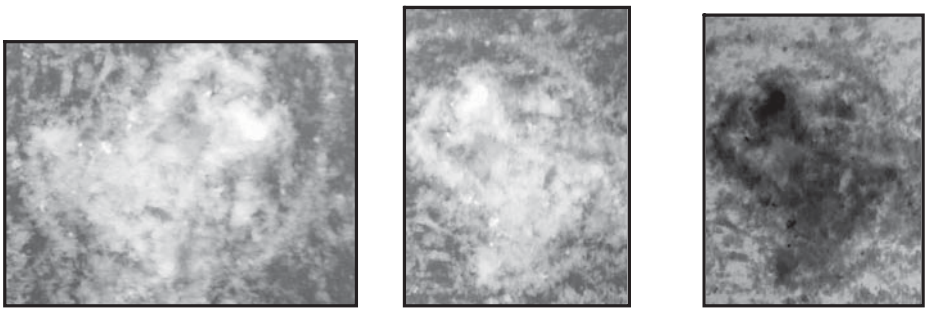

FIGURE 16 Three images of the same biofilm. A = original image; B = image rotated to the left; C = image reversed. For all images the textural parameters were the same (TE = 5.6547, E = 0.0052, H = 0.3656), showing that the textural parameters do not depend on the position or the microscopy technique used (reflected or transmitted).

TABLE VII The areal parameters calculated for the images in Figure 16

Image	AP	FD	ADD (pixel)	MDD (pixel)	AHRL (pixel)	AVRL (pixel)	P (pixel)
16A Original	0.473	1.231	20.386	85.586	53.293	50.170	8683
16B Rotated left	0.473	1.231	20.386	85.586	50.170	53.293	8683
16C Reversed	0.527	1.236	16.739	123.794	41.662	41.155	10286

binary image. Figure 17 shows the impact that threshold has on the calculation of biofilm areal porosity. Different operator preferences for the threshold doubled the estimate of biofilm AP in some cases.

Since there is no absolute measure of correctness for the threshold, it was determined that an acceptable automatic thresholding method should give a value approaching the average value determined by a panel of human experts (Xavier *et al*., 2001; Yang *et al*., 2001). It was assumed that an automatic procedure that has sufficient precision will yield more reproducible results than human operators. To evaluate the efficiency of selected automatic image thresholding procedures, the following were tested: i) the variability among thresholds set manually by different operators, ii) the variability of thresholds set automatically using known thresholding algorithms, and iii) the agreement between the thresholds set manually and automatically.

To the authors' knowledge, image thresholding algorithms have not been tested on biofilm images. Most thresholding algorithms described in the literature were based on measuring boundaries and edges, and were tested on objects having well-defined boundaries, such as microbes or fluorescent particles (see review paper by Wilkinson, 1998). Attempts were made to use these boundary- and edge-detecting algorithms for biofilm images. However, the cell clusters in biofilms do not have clearly marked boundaries and the applicability of these algorithms is questionable. Techniques that use entropy and histogram properties were focussed upon, and five methods of automatic thresholding available in the computer science literature were chosen: i) local entropy (Pal & Pal., 1989), ii) joint entropy (Pal & Pal., 1989), iii) relative entropy (Chang *et al*., 1994), iv) Renyi's entropy (Sahoo *et al*., 1997), and v) iterative selection (Ridler & Calvard, 1978).

The images of biofilms were generated by reflected light microscopy, transmission light microscopy, and confocal scanning laser microscopy (CSLM). To generate a reference set, ten researchers from the Center for Biofilm Engineering at MSU, manually thresholded the same images. The results of the different automatic thresholding procedures were compared with each other and with the results of manual thresholding. Only the iterative selection method was found satisfactory in that it consistently set the threshold level near that set manually.

The iterative selection method assumes that there is a mean value which is the optimal threshold value for both background and foreground pixels.

As seen in Figure 18 $t_{opt} = (t_{back} + t_{fore})/2$ must be calculated iteratively using the following algorithm: t_{back} = average of background pixels; t_{fore} = average of foreground pixels.

Iterative selection algorithm: i) select t_{opt}, called t_{optS}; ii) calculate $t_{opt} = (t_{back} + t_{fore})/2$; iii) if $t_{opt} = t_{optS}$ it is the correct threshold value; otherwise stop; iv) if $t_{opt} \neq t_{optS}$ go to step i).

The selection of t_{opt} is done starting from i) and continuing with increasing numbers until step iii) is satisfied.

Since image thresholding is subjective, the current version of ISA is equipped with two automatic thresholding options: iterative selection (Yang *et al*., 2001) and Otsu's method (Otsu, 1979).

Effect of Image Filtering

The filtering of digital images is the modification of individual pixels based on the properties of surrounding pixels. It is a common procedure in image manipulation and in image analysis, and it is reasonable to be concerned about the possible impact

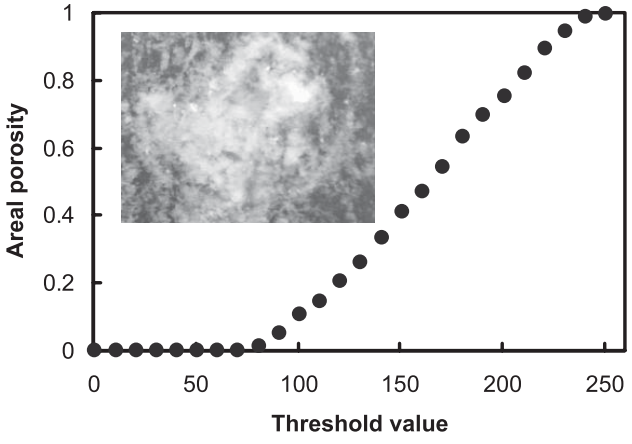

FIGURE 17 The gray scale biofilm image shown in the inset of the figure (previously presented as Figure 16A) was used to test variation in AP by threshold value. The AP was 0.1 and 0.4 for the gray scale thresholds of 100 and 150, respectively.

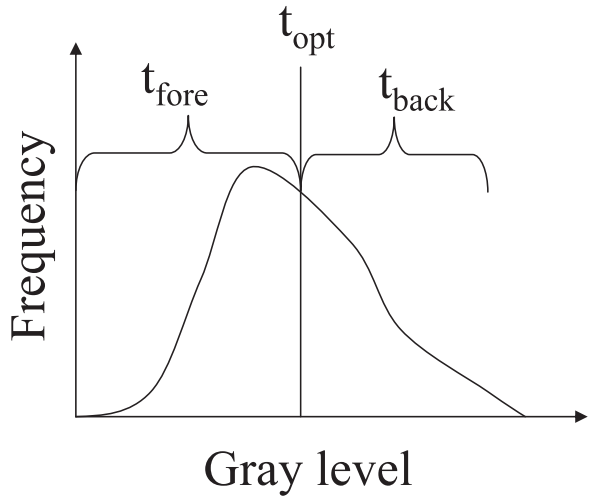

FIGURE 18 Schematic representation of optimum thresholding (t_{opt}) on a histogram. T_{fore} = average of foreground pixels and t_{back} = the average of background pixels.

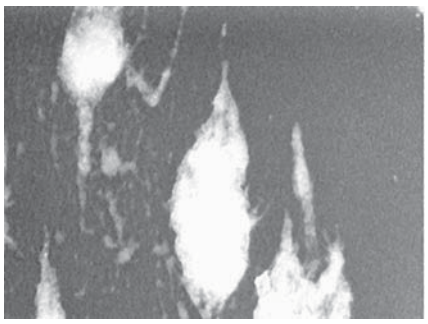

FIGURE 19 The biofilm image used to test the effect of filtering.

on computed textural and areal parameters. We used the biofilm image in Figure 19 to quantify the effect of image filtering on the textural and areal parameters. Median filtering was used, which is a nonlinear operation often used in image processing to reduce 'salt and pepper' noise. Median filtering is more effective than convolution when the goal is to simultaneously reduce noise and preserve edges (Lim, 1990; MATLAB® Version 6.5, Release 13, medfilt2 help file). MATLAB's built-in median filter (medfilt2(A,[m n]) was used to perform median filtering of matrix A (the image) in two dimensions. Each output pixel contained the median value in the m-by-n neighborhood around the corresponding pixel in the input image. A symmetric filter with m = n was used.

Effect of Image Filtering on Areal Parameters

This section evaluates the effect of filtering the biofilm images on the areal parameters computed from the image in Figure 19. The results are shown in Figure 20. All areal parameters were affected, although to different extents. A filter size of five pixels seems to be the largest that can be applied before the parameters start to be affected significantly. The mathematics of digital filtering shows significant changes at a size of five pixels, so this effect is not unexpected.

Effect of Image Filtering on Textural Parameters

A median filter (x,x) was applied to the biofilm image in Figure 19 and showed the effects of filtering on the textural parameters (Figure 21). The filter clearly affected the computed textural parameters. Energy increases logarithmically when the applied filter size is greater than one pixel in diameter. It follows from the one-pixel neighborhoods used to compute the GLCM that any filter with a size greater than one will have some effect on textural parameters. This effect should be taken into consideration when selecting the extent of filtration, particularly because there are no

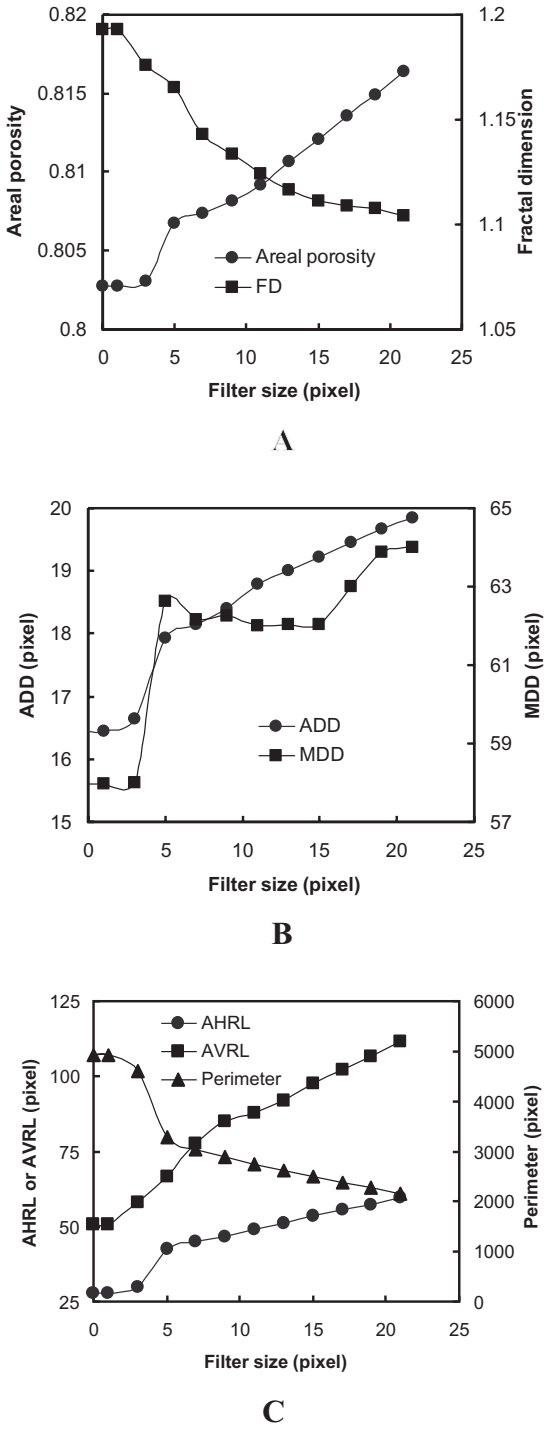

FIGURE 20 Effect of filter pixel size on the AP (A) and FD (B) ADD and MDD, and (C) average horizontal and vertical lengths and perimeter for the image given in Figure 19. The binary images were filtered using a median filter with filter size (x,x). The images were filtered after being thresholded.

algorithms to select the correct filter size for gray scale images and the filtering effect varies from one image to another. Therefore, it is important to report the type and the size of the filter used to manipulate the image before computing textural parameters.

Effect of Image Focus

Another important question frequently asked is whether image focusing affects the computed parameters. To quantify this effect, the lens was focussed on the bottom of the biofilm in Figure 22A to get the best focus. To decrease the image quality progressively, the focus was then changed to 100 μm and 200 μm below the best focus, and 100 μm and 200 μm above the best focus. The computed parameters are shown in Table VIII. Areal parameters varied predictably, and show maxima or minima at the best focus. However, textural entropy and homogeneity varied randomly without showing a trend. Visually there is little difference between these images. However, as seen in Table viii the computed parameters are different, showing that image quality is important and that it affects the computed parameters. For example, if two operators collect the same images but each focuses differently, they will compute different parameters.

Effects of Magnification

To quantify the effect of magnification on computed parameters, an image was taken at 100 × magnification (Figure 23A) and another image from the same location but using 40 × (Figure 23B). Of course, when the magnification changed, the coverage area changed also, so that the image in Figure 23B covers more area than that in Figure 23A. To evaluate the effects statistically 20 images of the same biofilm were taken using 100 × and 40 × magnification and the areal and textural parameters were computed. The results for the images in Figure 23 are shown in Table IX, and the results for the other 20 images of the same biofilm along with the statistical analysis are shown in Table X.

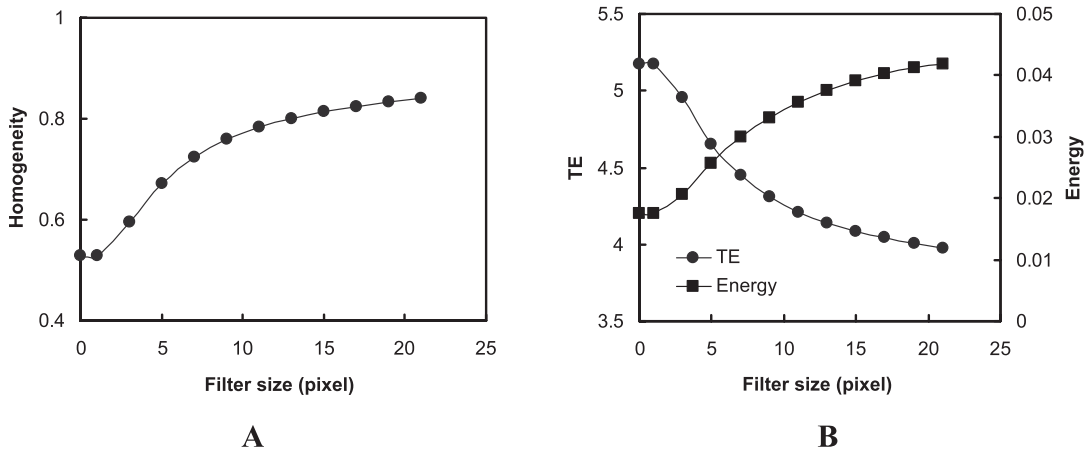

FIGURE 21 Effect of filter pixel size on H (A) and TE and E (B). In the figure the filter size shows the value of x. The applied filter size is [x,x].

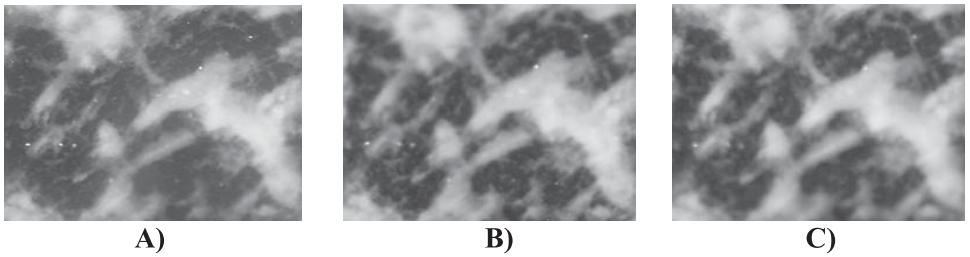

FIGURE 22 The same biofilm image but focused differently. A = focused at the bottom; B = focused 100 μm below the bottom; C = focused 100 μm above the bottom. Visually, the images look similar, but the areal parameters differ.

TABLE VIII Structural parameters computed from images collected at the same location but focused differently

Position (μm)	AP	FD	ADD (pixels)	MDD (pixels)	HRL (pixels)	VRL (pixels)	P (pixels)	E	TE	H
− 200	0.578265	1.21822	20.94607	81.32035	55.64308	39.89537	7357	0.001835	6.806218	0.392095
− 100	0.56242	1.20777	19.14667	80.61017	52.791	38.40468	8141	0.001576	7.034068	0.355179
0	0.641921	1.21487	17.8444	76.48529	45.33151	30.14895	7971	0.001957	6.784296	0.364352
100	0.580937	1.17529	19.02531	82.73452	57.20146	40.79987	7222	0.001641	7.00746	0.360304
200	0.59367	1.20722	21.39081	81	59.1484	41.58336	6806	0.001854	6.823609	0.391096

These results show that image magnification affects some of the parameters but not others. To quantify the effect of image magnification, the ratio (R) of the value the parameter had at 100 × to the value it had at 40 × was used. In cases where the image magnification is not critical, R = 1. Table X shows results obtained from the analysis of 20 images of the same biofilm acquired using 40 × and 100 × magnifications.

For AP and TE R is close to 1, showing that these parameters are not greatly affected by the magnification. R was slightly lower for FD, MDD, AHRL, AVRL, P, E, and H, showing that these parameters are slightly affected by magnification. ADD was the most affected parameter: R = 3.24. Since in some cases R was close to but not exactly equal to 1, the t-test was used to compute the statistical significance of these data and *p* values computed using the null hypothesis showed that the parameters were identical at the 5% level of significance (Martinez & Martinez, 2002).

The results in Table X show that AP and TE do not depend on image magnification. Other than areal porosity, the areal parameters depend on the magnification. Using 100 × magnification, more detail can be seen in the image, such as small cell clusters, which are not seen with 40 × . The most important conclusion from the results shown in Table X is that when comparing images of different biofilms it is critical to use the same magnification.

Effect of Illumination Intensity on AP

As expected the intensity of the light used to illuminate the biofilms affects the calculated AP. This effect is especially significant when biofilms are highly illuminated. Increased light intensity makes more areas visible in the biofilm; however it also increases fluorescent light emitted by the biofilm, which causes bleaching. According to the authors' experience, the effect of light intensity decreased with decreased AP since there was enough biofilm to reflect the light (see Figure 24).

CONCLUSIONS

Several parameters quantifying structural features of biofilms can be computed from biofilm images, *viz.* AP, ADD, MDD, AHRL and AVRL, P, TE, E and H.

From the authors' studies, the most useful areal parameters for quantifying biofilm structure are AP and ADD, probably because their meaning is intuitively clear and they have a direct relation to biofilm processes. The most useful textural parameter is found to be TE, which can be used to compare images of different biofilms. However, this conclusion may not apply to all biofilms. Therefore, calculating all parameters is suggested and then choosing the most appropriate parameter using statistical analysis.

Comparing biofilm images is not a precise science, and the procedures employed are often difficult to standardize. Attempting to compare images of biofilms it is imperative to observe simple rules: i) It is important to use good quality images to quantify biofilm structure and to use a consistent procedure to acquire these images. This is particularly important when comparing data collected by different operators who may, for

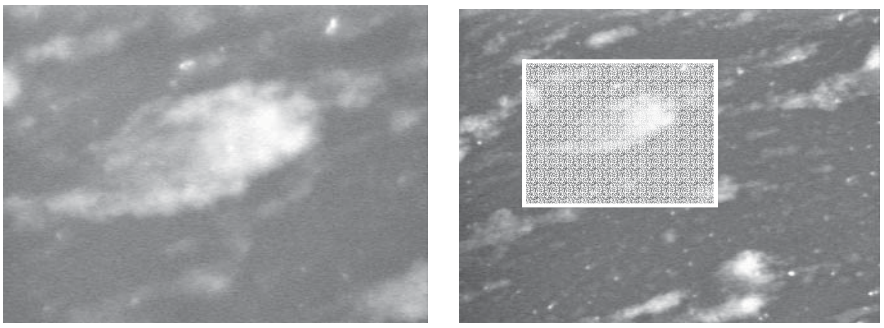

FIGURE 23 A = an image using 100 × magnification; B = an image of the same location using 40 × . Note image B covers more area compared to image A. The cell cluster in image A is marked in image B.

TABLE IX The structural parameters computed from the images in Figure 23

	AP	FD	ADD (μm)	MDD (μm)	AHRL (μm)	AVRL (μm)	P (μm)	E	TE	H
40 ×	0.85021	1.2788	6.053965	40.388	15.109	7.760388	16477.5	0.02239	4.50579	0.3277972
100 ×	0.79535	1.4273	6.70264	34.9285	9.85085	4.70217	5905	0.01781	4.65018	0.3452019
Ratio = R (100 × /40 ×)	0.93	1.12	1.107149	0.8648	0.65198	0.605919	0.358367	0.795	1.03	1.05

TABLE X The structural parameters computed from 20 images of the same biofilm acquired using 40 × and 100 × magnifications; level of significance = 0.05

	AP	FD	ADD (μm)	MDD (μm)	AHRL (μm)	AVRL (μm)	P (μm)	E	TE	H
40 × −average	0.8071	1.319	26.4	78.2125	29.83875	14.65415	12565	0.01732	4.83272	0.343235
SD	0.0578	0.043	5.94125	26.9625	11.22263	5.781558	4157.5	0.00468	0.22892	0.013783
100 × −average)	0.7589	1.421	3.2605	43.955	14.9795	6.51836	5354	0.01849	4.72513	0.369305
SD	0.101	0.078	2.988	13.665	4.9531	2.188209	2616.5	0.00537	0.19683	0.032455
p-value	0.0718	< 0.0001	< 0.0001	< 0.0001	< 0.0001	< 0.0001	< 0.0001	0.4671	0.1193	0.0021
Comment	This difference is statistically to be not significant	this difference is statistically significant	This difference is statistically significant	This difference is statistically significant	This difference is statistically significant	This difference is statistically significant	this difference is statistically significant	this difference is not statistically significant	this difference is significant	this difference is significant
Ratio = R (100 × / 40 ×)	1.07	0.93	3.24	0.71	0.80	0.90	0.94	0.94	1.03	0.93

example, focus differently. ii) It is important that the compared images be taken at the same magnification. For any given biofilm image, changing magnification changes structural parameters to some extent. In the example given, ADD was the parameter most critically affected by varying magnifications. iii) It is important to use the same type and size of filter applied to the analyzed image (and to report these factors). Specifically, thresholding changes the numerical values of the areal parameters, and without knowing the effect of filtering, the information conveyed by the parameters is much less useful.

The possible uses of parameters computed from biofilm images are to i) compare structures of different biofilms; ii) test the reproducibility of biofilm structure; iii) monitor temporal variations in biofilm structure; iv) test the effects of various substances, including antimicrobials, on biofilm structure; v) quantify effects of environmental factors on biofilm structure; and vi) extract parameters for biofilm modeling.

Useful information from structural parameters comes from comparing image sets taken at different times. Each set of experiments has its own characteristics, and it is meaningless to compare structural data computed from images acquired using different lighting, filtering, and magnification.

The analysis of biofilm structure is most pertinent when used to monitor temporal variations, and it is least pertinent when used to compare biofilms accumulated in different reactors, in different laboratories, and/or grown under different environmental conditions. Thus, image analysis of biofilm is a useful tool for monitoring the temporal development of biofilms, but it appears to be less useful as a base for general conclusions about the nature of biofilm processes.

Although there has been considerable effort devoted to analysis of biofilm structure, it is still not clear which parameters are relevant, or which of the biofilm processes these parameters reflec. It is one thing to calculate these parameters, and another thing to know what they mean. To illustrate this point several structural parameters were computed from an image of the authors' own research group (Figure 25). The results are in Table XI.

ABBREVATIONS

ADD Average diffusion distance
AHRL Average horizontal run length
AP Areal porosity
AVRL Average vertical run length
E Energy

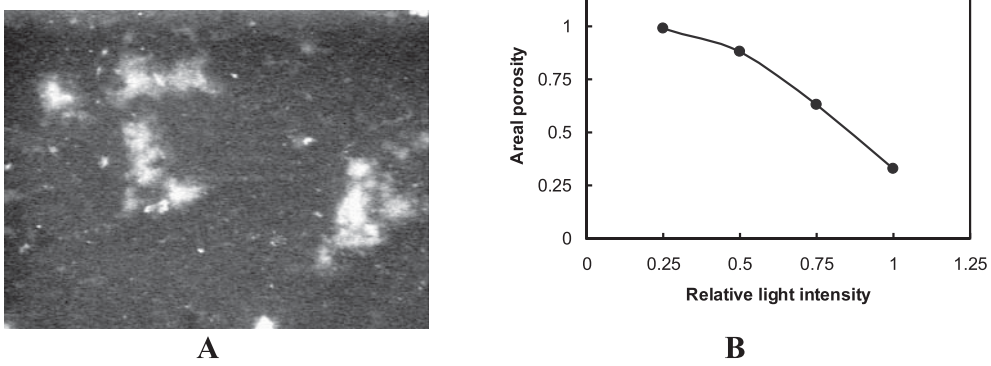

FIGURE 24 Effect of relative light intensity on calculated AP values. Relative light intensity was calculated as the ratio between applied light power to maximum light power. The image in A was acquired using reflected light microscopy.

TABLE XI The structural parameters computed from Figure 25

Porosity	FD	ADD (pixels)	MDD (pixels)	AHRL (pixels)	AVRL (pixels)	P (pixels)	E	TE	H
0.42	1.51	33.94	230.15	27.61	27.88	110578	0.00084	7.999	0.397

FIGURE 25 Biofilm Structure and Function Research Group. This image was used to calculate structural parameters and present the results shown in Table XI.

FD	Fractal dimension
H	Homogeneity
MDD	Maximum diffusion distance
P	Perimeter
SD	Standard deviation from the average
TE	Textural entropy

Acknowledgements

The work was supported by grant N-00014-02-1-0567 from the US Office of Naval Research, grants DE-FG03-01ER63270 and DE-FG03-98ER62630/A001 from the Natural and Accelerated Bioremediation Research (NABIR) program, and by Biological and Environmental Research (BER) and the US Department of Energy.

References

Beyenal H, Lewandowski Z (2000) Combined effect of substrate concentration and flow velocity on effective diffusivity in biofilms. *Water Res* **34:** 528–538

Beyenal H, Lewandowski Z (2001) Mass transport dynamics, activity, and structure of sulfate reducing biofilms. *AIChE* **47:** 1689–1697

Beyenal H, Lewandowski Z (2002) Internal and external mass transfer in biofilms grown at various flow velocities. *Biotechnol Prog* **18:** 55–61

Beyenal H, Tanyolaç A, Lewandowski Z (1998) Measurement of local effective diffusivity and cell density variations in heterogeneous biofilms. *Water Sci Technol* **38:** 171–178

Bishop P L (1997) Biofilm structure and kinetics. *Water Sci Technol* **36:** 287–294

Bishop P L, Rittmann B E (1995). Modelling heterogeneity in biofilms: report of the discussion session. *Water Sci Tech*nol **32:** 263–265

Breu H, Gil J, Kirkpatrick D, Werman M (1995) Linear time euclidean distance transform algorithms. *IEEE Trans Pattern Anal Machine Intell* **17:** 529–533

Caldwell D E, Korber D R, Lawrence J R (1992) Imaging of bacterial cells by fluorescence exclusion using scanning confocal laser microcopy. *J Microbiol Methods* **15:** 249–263

Chang C I, Chen K, Wang J, Althouse M L G (1994) A relative entropy-based approach to image thresholding. *Pattern Recogn* **27:** 1275–1289

Christensen B E, Ertesvag H, Beyenal H, Lewandowski Z (2001) Resistance of biofilms containing alginate-producing bacteria to disintegration by an alginate degrading enzyme (AlgL). *Biofouling* **17:** 203–210

Daims H, Ramsing N B, Schleifer K H, Wagner M. (2001) Cultivation-independent, semiautomatic determination of absolute bacterial cell numbers in environmental samples by fluorescence *in situ* hybridization. *Appl Environ Microbiol* **67:** 5810–5818

deBeer D, Stoodley P, Lewandowski Z (1994b) Liquid flow in heterogeneous biofilms. *Biotechnol Bioeng* **44:** 636–641

deBeer D, Stoodley P, Roe F, Lewandowski Z (1994a). Effects of biofilm structures on oxygen distribution and mass transport. *Biotechnol Bioeng* **43:** 1131–1138

Dionisi H M, Layton A C, Robinson K G, Brown J R, Gregory I R, Parker J J, Sayler G S (2002) Quantification of *Nitrosomonas oligotropha* and *Nitrospira* spp. using competitive polymerase chain reaction in bench-scale wastewater treatment reactors operating at different solids retention times. *Water Environ Res* **74:** 462 – 469

Haralick R M, Shanmugam K, Dinstein I (1973). Textural features for image classification. *IEEE Trans Sys Man Cyber* SMC-3 **6:** 610 – 621

Hermanowicz S W (2001) A simple 2D biofilm model yields a variety of morphological features. *Math Biosci* **169:** 1 – 14

Hermanowicz S W, Schindler U, Wilderer (1995). Fractal structure of biofilms: new tools for investigation of morphology. *Water Sci Technol* **32:** 99 – 105

Heydorn A, Ersboll BK, Hentzer M, Parsek M R, Givskov M, Molin S (2000b) Experimental reproducibility in flow-chamber biofilms. *Microbiology (Reading)* **146:** 2409 – 2415

Heydorn A, Nielsen A T, Hentzer M, Sternberg C, Givskov M, Ersboll B K, Molin S, (2000a) Quantification of biofilm structures by the novel computer program COMSTAT. *Microbiology (Reading)* **146:** 2395 – 2407

Heydorn A, Ersboll B, Kato J, Hentzer M, Parsek M R, Tolker-Nielsen T, Givskov M, Molin S (2002) Statistical analysis of *Pseudomonas aeruginosa* biofilm development: impact of mutations in genes involved in twitching motility, cell-to-cell signaling, and stationary-phase sigma factor expression. *Appl Environ Microbiol* **68:** 2008 – 2017

Jackson G, Beyenal H, Rees W M, Lewandowski Z (2001) Growing reproducible biofilms with respect to structure and viable cell counts. *J Microbiol Methods* **47:** 1 – 10

Ji Z, Heydorn A, Molin S, Mathee K, Narasimhan G (2000) Quantitative analysis of *Pseudomonas aeruginosa* biofilm images using fractal dimensions. ASM Biofilms Big Sky, MT July 16 – 20

Kaandorp J (1994) *Fractal Modeling Growth and Form in Biology*. Springer Verlag, Berlin

Kjelleberg S, Molin S (2002) Is there a role for quorum sensing signals in bacterial biofilms? *Curr Opin Microbiol* **5:** 254 – 258

Kuehn M, Hausner M, Bungartz HJ, Wagner M, Wilderer PA, Wuertz S (1998) Automated confocal laser scanning microscopy and semiautomated image processing for analysis of biofilms. *Appl Environ Microbiol* **64:** 4115 – 4127

Lawrence J R, Korber D R, Hoyle B D, Costerton J W, Caldwell D E (1991) Optical sectioning of microbial biofilms. *J Bacteriol* **173:** 6558 – 6567

Lewandowski Z (2000) Notes on biofilm porosity. *Water Res* **34:** 2620 – 2624

Lewandowski Z, Stoodley P (1995) Flow induced vibrations, drag force, and pressure drop in conduits covered with biofilm. *Water Sci Technol* **32:** 19 – 26

Lewandowski Z, Beyenal H (2003a) Biofilm monitoring: a perfect solution in search of a problem. *Water Sci Technol* **47:** 1251 – 1256

Lewandowski Z, Beyenal H (2003b) Mass transfer in heterogeneous biofilms. In: Wuertz S, Bishop P L, Wilderer P A (eds) *Biofilms in Wastewater Treatment*. IWA Publishing, London, pp 145 – 172

Lewandowski Z, Altobelli S A, Fukushima E (1993a) NMR and microelectrode studies of hydrodynamics and kinetics in biofilms. *Biotechnol Prog* **9:** 40 – 45

Lewandowski Z, Beyenal H, Stookey D (2004) Reproducibility of biofilm processes and the meaning of steady state in biofilm reactors. *Water Sci Technol* (In press)

Lewandowski Z, Stoodley P, Altobelli S, Fukushima E (1993b) Hydrodynamics and kinetics in biofilm systems - recent advances and new problems. *Proc 2nd* IAWQ Int *Specialized Conf Biofilm Reactors*,1993. Paris, France, pp 313 – 319

Lewandowski Z, Webb D, Hamilton M, Harkin G (1999) Quantifying biofilm structure. *Water Sci Technol* **39:** 71 – 76

Lim J S (1990) *Two-Dimensional Signal and Image Processing*. Prentice Hall, Englewood Cliffs, NJ, pp 469 – 476

Lomander A, Schreuders P, Russek-Cohen E, Ali L (2002) A method for rapid analysis of biofilm morphology and coverage on glass and polished and brushed stainless steel. *Trans ASAE* **45:** 479 – 487

Martinez W L, Martinez A R (2002) *Computational Statistics Handbook with MATLAB®*. Chapman & Hall/CRC, Boca Raton, Florida, USA, 195 pp

Mah T-F, Pitts B, Pellock B, Walker G C, Stewart P S, O'Toole G A (2003) A genetic basis for *Pseudomonas aeruginosa* biofilm antibiotic resistance. *Nature* (*Lond*) **426:** 306 – 310

Otsu N (1979) A threshold selection method from gray-level histograms. *IEEE Trans Systems, Man, Cybernetics* **9:** 62 – 66

Pal N R, Pal S K (1989) Entropy thresholding. *Signal Process* **16:** 97 – 108

Pereira M O, Kuehn M, Wuertz S, Neu T, Melo L F (2002) Effect of flow regime on the architecture of a *Pseudomonas fluorescens* biofilm. *Biotechnol Bioeng*. **78:** 164 – 171

Picioreanu C, van Loosdrecht M C M, Heijnen J J (1998a) A new combined differential-discrete cellular automaton approach for biofilm modeling: application for growth in gel beads. *Biotechnol Bioeng* **57:** 718 – 731

Picioreanu C, van Loosdrecht M C M, Heijnen J J (1998b) Mathematical modeling of biofilms structure with a hybrid differential-discrete cellular automaton approach. *Biotechnol Bioeng* **58:** 101 – 116

Picioreanu C, van Loosdrecht M C M, Heijnen J J (2000) Effect of diffusive and convective substrate transport on biofilm structure formation: a two-dimensional modeling study. *Biotechnol Bioeng* **69:** 504 – 515

Picioreanu C, van Loosdrecht M C M, Heijnen J J (2001) Two-dimensional model of biofilm detachment caused by internal stress from liquid flow. *Biotechnol Bioeng* **72:** 205 – 218

Purevdorj B, Costerton J W, Stoodley P (2002) Influence of hydrodynamics and cell signaling on the structure and behavior of *Pseudomonas aeruginosa* biofilms. *Appl Environ Microbiol* **68:** 4457 – 4464

Ridler T W, Calvard S (1978) Picture thresholding using an iterative selection method. *IEEE Trans Systems, Man. Cybernetics*. **SMC-8:** 630 – 632

Rittmann B R, Pettis M, Reeves W H, Stahl D (1999) How biofilm clusters affect substrate flux and ecological selection. *Water Sci Technol* **39:** 99 – 105

Russ J (2002) *The Image Processing Handbook*. CRC Press, Boca Raton, FL, USA, pp 515 – 519

Sahoo P, Wilkins C, Yeager J (1997) Threshold selection using Renyi's entropy. *Pattern Recogn* **30:** 71 – 84

Shannon C E (1948) A mathematical theory on communication. *Bell System Tech J* **27:** 379 – 423

Tanyolaç A, Beyenal H (1997) Prediction of average biofilm density and performance of a spherical particle under substrate inhibition. *Biotechnol Bioeng* **56:** 319 – 329

van Loosdrecht M C M, Heijnen J J, Eberl H, Kreft J, Picioreanu C (2002) Mathematical modeling of biofilm structures. *Antonie Leeuwenhoek* **81:** 245 – 256

van Loosdrecht M C M, Eikelboom D, Gjaltema A, Mulder A, Tijhuis L, Heijnen J J (1995). Biofilm structures. *Water Sci Technol* **32:** 35 – 43

Wilkinson M H F (1998) Automated and manual segmentation techniques in image analysis of microbes. In: Wilkinson M H F, Schut F (eds) *Digital Image Analysis: Imaging, Morphometry, Fluorometry and Motility Techniques and Applications*. John Wiley and Sons, 135 – 171

Wimpenny J W, Colasanti R (1997) A unifying hypothesis for the structure of microbial biofilms based on cellular automaton models. *FEMS Microbiol Ecol* **22:** 1 – 16

Xavier J B, Schnell A, Wuertz S, Palmer R, White D C, Almeida J S (2001) Objective threshold selection procedure (OTS) for segmentation of scanning laser confocal microscope images. *J Microbiol Methods* **47:** 169 – 180

Yang S, Lewandowski Z (1995) Measurement of local mass transfer coefficient in biofilms. *Biotechnol Bioeng* **48:** 737 – 744

Yang X, Beyenal H, Harkin G, Lewandowski Z (2000) Quantifying biofilm structure using image analysis. *J Microbiol Methods* **39:** 109 – 119

Yang XM, Beyenal H, Harkin G, Lewandowski Z (2001) Evaluation of biofilm image thresholding methods. *Water Res* **35:** 1149 – 1158

Zahid W M, Ganczarczyk J J (1994) Fractal properties of the RBC biofilm structure. *Water Sci Technol* **29:** 271 – 279

Zhang T C, Bishop P L (1994) Evaluation of tortuosity factors and effective diffusivities in biofilms. *Water Res* **28:** 2279 – 2287